INFRARED DIELECTRIC CHARACTERISTICS OF POROUS BINARY AND TERNARY III-NITRIDES HETEROSTRUCTURES

PAULINE YEW

UNIVERSITI SAINS MALAYSIA

2018

INFRARED DIELECTRIC CHARACTERISTICS OF POROUS BINARY AND TERNARY III-NITRIDES HETEROSTRUCTURES

by

PAULINE YEW

Thesis submitted in fulfillment of the requirements
for the degree of
Doctor of Philosophy

August 2018

ACKNOWLEDGEMENT

I would like to express my gratitude to my main supervisor, Assoc. Prof. Dr. Ng Sha Shiong for his invaluable guidance, patience and tolerance throughout the research. His full support definitely facilitates the progress of this work. Secondly, I would like to acknowledge my co-supervisor, Prof. Dr. Haslan Abu Hassan. I am undoubtedly enlightened with his constructive advices and positive attitude towards education. Thirdly, I would like to thank my second co-supervisor, Assoc. Prof. Dr. Yoon Tiem Leong for sharing his knowledge and idea in solving mathematical problems.

A special thank is reserved for my senior, Dr. Lee Sai Cheong, who not only guides me professionally throughout the entire research but also instills positive research attitude in me. Besides, I would like to express my appreciation to other members of my research team and other post-graduate students who are working in the same laboratory. I sincerely thank to all lab assistants in the School of Physics and Institute of Nano Optoelectronics Research and Technology (INOR) for their assistance in experimental works.

Thanks to the very first collaborator who involved in this dissertation, Prof. Dr. Chen Wei Li from National Changhua University of Education who provides flat wurtzite InGaN thin films as well as the assistance in reciprocal space mapping measurements. Thanks to Prof. Dr. Thomas Osipowicz and Dr. Minqin Ren from National University of Singapore for their help in determining the composition of the porous InGaN samples.

I am indebted to the Ministry of Higher Education of Malaysia for offering me MybrainSc scholarship to reduce my financial burden during my research study. The support from TWAS Research Grant Programme (Grant No. 11-120 RG/MSN/AS_C: UNESCO FR: 3240262655) and Fundamental Research Grant Scheme of Ministry of Higher Education Malaysia (FRGS Grant No. 203/PFIZIK/6711282) is also greatly appreciated. In addition, I would like to express gratitude to The Abdus Salam International Centre for Theoretical Physics (ICTP) for giving me opportunity to participate the Hands-On Research Training Programme in Complex Systems at Trieste ICTP campus, Italy. Thanks to the SAKURA exchange programme for offering me the opportunity to visit Tokyo City University, Japan and to interact with their researchers. These programmes indeed widen my horizon and leave huge beneficial impacts on my scientific thinking construction.

Last but not least, I would like to express my greatest thanks to my beloved family and friends who give me their continuous encouragement and support to complete my research.

TABLE OF CONTENTS

LIST OF TABLES

LIST OF FIGURES

LIST OF ABBREVIATIONS

A-BG	Asymmetric-Bruggeman
ATR	Attenuated total reflectance
BG	Bruggeman model
EMT	Effective medium theory
EM	Electromagnetic wave
ER	Electrostatic resonance
FESEM	Field-emission electron microscope
FDTD	Finite-difference time-domain method
FEM	Finite element method
FD	First derivative
FTIR	Fourier transform infrared
GUI	Graphical user interface
IR	Infrared
ISB	Intersubband
Inv-MG	Inverse Maxwell Garnett
LTNK	Lichtenecker model
LO	Longitudinal optical

LOPC	Longitudinal optical phonon-plasmon coupling
LPP	Longitudinal plasmon-phonon mode
Loo	Looyenga model
MG	Maxwell Garnett model
MREI	Modified random element isodisplacement
MBE	Molecular beam epitaxy
NN	Nearest neighbour
n-GaN	n-type GaN film layer
c-axis	Optic axis
FDTD	Periodic finite-difference time-domain
PGaN	Porous GaN
PL	Power law
PIXE	Proton Induced X-ray Emission
REI	Random element isodisplacement
Ra	Rayleigh
Ref	Reference
SN	Sample normal
SNN	Second nearest neighbour

nGaN	Si-doped GaN/*c*-sapphire heterostructure
SPhP	Surface phonon polariton
SPP	Surface plasmon polariton
THz	Terahertz
3D	Three-dimension
TE	Transverse electric (*s*-polarization)
TM	Transverse magnetic (*p*-polarization)
TO	Transverse optical
2D	Two-dimension
UV	Ultraviolet
u-GaN	Undoped GaN film layer
UID	Unintentionally doped

LIST OF SYMBOLS

ω	Angular frequency
τ	Averaged relaxation time of the charge carriers
n_{bound}	Bound charge density
n	Charge carrier density
b_{ij}	Coefficient (MREI model)
ε	Complex dielectric function
x	Composition
Θ	Constant (MREI model)
g	Constant for wurtzite crystal (MREI model)
γ	Damping
γ_b	Damping constant of bound electron
N_p	Depolarization factor
ε_{bound}	Dielectric contribution due to the bound electron
ε_{free}	Dielectric contribution due to the free electron
ε_{ion}	Dielectric contribution due to the lattice ion
$\varepsilon_{\parallel}$	Dielectric function component which is parallel to the *c*-axis
$\varepsilon_{\perp}$	Dielectric function component which is perpendicular to the *c*-axis

ε_m	Dielectric function of host
ε_1	Dielectric function of incident the incident medium
ε_i	Dielectric function of inclusion
a	Dimension of the inclusion
$\boldsymbol{D}$	Displacement field
$\boldsymbol{u}_A$	Displacement of ion A from equilibrium positions
$\boldsymbol{u}_B$	Displacement of ion B from equilibrium positions
$\boldsymbol{u}_C$	Displacement of ion C from equilibrium positions
$<\boldsymbol{D}>$	Effective electric displacement field
$<\boldsymbol{E}>$	Effective electric field
m^*	Effective electron mass
ε_{eff}	Effective permittivity
λ_{eff}	Effective wavelength of the radiation in the composite
e	Electric charge
$D_z(z)$	Electric displacement field component along z direction
$E_x(z)$	Electric field component along x direction
$\boldsymbol{E}_1$	Electric field in material 1
$\boldsymbol{E}_2$	Electric field in material 2

$\boldsymbol{E}_{\mathrm{i}}$	Electric field inside the inclusion
$\boldsymbol{E}_{\mathrm{m}}$	Electric field outside the inclusion (or in the host medium)
m_{e}	Electron mass
$\boldsymbol{E}_{\mathrm{e}}$	External electric field
d_{IR}	Film thickness which is probed using IR reflectance spectroscopy
F_{BC0}	Fitting force constants between BC ion pairs
F_{AB}	Force constants between AB ion pairs
F_{AB0}	Force constants between AB ion pairs in pure binary AB crystal
F_{AC}	Force constants between AC ion pairs
F_{AC0}	Force constants between AC ion pairs in pure binary AC crystal
F_{BC}	Force constants between BC ion pairs
n_{free}	Free electron charge density
ω_{F}	Fröhlich mode
ε_{G}	Gervais dielectric model
γ_{G}	Grüneisen parameter
ω_0	Harmonic frequency of the phonon mode
ε_∞	High frequency dielectric constant
ε”	Imaginary part of the dielectric function

$\omega_{\mathrm{ImB,\ AC}}{}^2$	Impurity mode arise due to the infinitely diluted impurity B in binary crystal AC
$\omega_{\mathrm{ImC,\ AB}}{}^2$	Impurity mode arise due to the infinitely diluted impurity C in binary crystal AB
θ	Incident angle
β	Index describes the transition from lowest bound's anisotropy to highest bound anisotropy
l	Index of layer
p_{ind}	Induced dipole moment
ϵ_{xx} or ϵ_{yy}	In-plane strain
l'	Integer value for spherical Bessel and Hankel functions
ε_{K}	Kukharskii dielectric model
a_L (c_L)	Lattice constant $a(c)$
γ_{LO}	LO damping constant
ω_{LO}	LO phonon mode
$\boldsymbol{E}_{\mathrm{loc}}$	Local electric field
γ_{LPP}	LPP damping constant
ω_{LPP}	LPP mode
$\boldsymbol{E}$	Macroscopic electric field
$\boldsymbol{H}$	Magnetic field
$\boldsymbol{B}$	Magnetic flux density

m_A	Mass of ion A
m_B	Mass of ion B
m_C	Mass of ion C
μ'	Mobility of carriers
v	Model parameter (Unified mixing model)
v'	Modified model parameter (Unified mixing model)
ϵ_{zz}	Out-of plane strain
K	Parallel (tangential) component of the wavevector with respect to the interface
ε_1	Permittivity of material 1
ε_2	Permittivity of material 2
q	Perpendicular (normal) component of wavevector with respect to the interface
a_{PDP}	Phonon deformation potential
b_{PDP}	Phonon deformation potential
$\Delta\omega_d$	Phonon mode shift due to anharmonic coupling to phonons of other branches
$\Delta\omega_s$	Phonon mode shift due to residual strain
$\Delta\omega_e$	Phonon mode shift due to thermal expansion
γ_p	Plasmon damping constant
ω_p	Plasmon frequency

α_e	Polarizability due to the displacement of electron cloud
α_i	Polarizability due to the displacement of ionic charges
$\boldsymbol{P}$	Polarization
$\boldsymbol{r}$	Position vector
R_p	*P*-polarized IR reflectivity
r_p	*P*-polarized reflection coefficient
R	Radius of spherical crystal
Z	Ratio of nearest neighbour (NN) force constant to second nearest neighbour (SNN) force constant
ε'	Real part of the dielectric function
μ_{AB}	Reduced mass of AB ion pair
μ_{AC}	Reduced mass of AC ion pair
n_p	Refractive index of ATR prism
$a_L{}^R$ ($c_L{}^R$)	Relaxed reference value of lattice constant a(c)
ω_b	Resonant frequency of bound electron
δ	Skin depth
c	Speed of light
R_s	*S*-polarized IR reflectivity
r_s	*S*-polarized reflection coefficient

ε_0	Static dielectric constant
σ	Stress
α_{AB}	Sum of the electronic polarizabilities of ions A and B
α_{AC}	Sum of the electronic polarizabilities of ions A and C
χ_{bound}	Susceptibility due to bound electron
e_{AB}	Szigeti-effective charges of binary members AB
e_{AC}	Szigeti-effective charges of binary members AC
α_c(T)	Temperature dependent thermal expansion coefficient parallel to the *c*-axis
α_a(T)	Temperature dependent thermal expansion coefficient perpendicular to the *c*-axis
d	Thickness of the film
γ_{TO}	TO damping constant
ω_{TO}	TO phonon mode
N	Total layer of heterostructure
N'	Total number of phonon oscillator
M'	Total number of plasmon oscillator
s	Total number of the cations in the multinary crystal
d_{FESEM}	Total thickness of a layer which is measured from one visible boundary to another in FESEM image
f_{air}	Volume fraction of the air

f	Volume fraction of the inclusion
f_1	Volume fraction of the material 1
f_2	Volume fraction of the material 2
V	Volume of the unit-cell for mixed crystal $A_xB_{1-x}N$
k	Wavevector
k_v	Wavevector of light in a vacuum
k_p	Wavevector of the incident light in a prism
k_x	Wavevector of SPhP along x direction

LIST OF APPENDICES

SIFAT DIELEKTRIK INFRAMERAH HETEROSTRUKTUR III-NITRIDA PERDUAAN DAN PERTIGAAN BERLIANG

ABSTRAK

Kebersandaran fungsi dielektrik inframerah (IR) ke atas keliangan dan komposisi bagi III-nitrida wurtzit telah dikaji secara teori dan eksperimen. Campuran 'seperti-ampaian' (GaN berliang) dan campuran 'seperti-larutan' ($In_xGa_{1-x}N$) digunakan untuk mengkaji kebersandaran fungsi dielektrik IR ke atas keliangan dan komposisi masing-masing. Walaupun banyak model medium berkesan (EMTs) boleh didapati daripada literatur, pemilihan EMT yang sesuai untuk menerangkan tindak balas berkesan bagi campuran 'seperti-ampaian' adalah mencabar dan masih tidak jelas. Oleh yang demikian, kajian mengenai dua-komponen campuran yang mempunyai empat jenis kombinasi fungsi dielektrik telah dijalankan. Satu garis panduan komprehensif yang bertujuan memilih EMT yang boleh menjelaskan tingkah-laku dielektrik berkesan bagi campuran 'seperti-ampaian' telah dicadangkan. Seterusnya, spektrum pantulan IR terkutub bagi satu set sampel GaN berliang (PGaN) dilakukan untuk mengkaji EMT terbaik yang menerangkan sistem PGaN serta kesan keliangan ke atas fungsi dielektrik berkesan. Spektrum pantulan PGaN boleh dijelaskan sepenuhnya oleh model faktor-Rayleigh (Ra) yang dikembangkan buat pertama kalinya untuk mengira lembapan mod Fröhlich. Dua mod Fröhlich yang lemah telah dikesan dalam spektrum pemantulan IR terkutub-*s* bagi PGaN pada 710 cm^{-1} dan 730 cm^{-1}. Ini menunjukkan bahawa dua polariton fonon permukaan (SPhP) tambahan dijangka muncul dalam spektrum pantulan penuh dikecilkan IR terkutub-*p* bagi PGaN. Selain itu, anjakan SPhP PGaN ke arah gelombang yang lebih rendah boleh diramalkan oleh model faktor-Ra semasa keliangan meningkatkan. Kebersandaran tingkah laku fonon optik ke atas komposisi disahkan dengan

menggunakan $In_xGa_{1-x}N$ wurtzit/heterostruktur-*c* nilam yang mempunyai dua jenis morfologi permukaan, iaitu rata dan berliang. Mod getaran kekisi E_1 yang diekstrak dari $In_{0.92}Ga_{0.08}N$ yang rata bersetuju dengan ramalan model elemen rawak isosesaran diubahsuai (MREI). Bagi wurtzite ternar $In_xGa_{1-x}N$ (x = 0.174, 0.477, 0.719 dan 0.883) yang berliang, ramalan MREI tentang fonon optik melintang bersetuju dengan data eksperimen. Persetujuan ini menunjukkan bahawa model MREI yang hanya mengambil kira interaksi jiran terdekat sudah mampu menggambarkan kebersandaran mod phonon optik ke atas komposisi bagi kristal bercampur, $In_xGa_{1-x}N$. Di samping itu, keputusan menunjukkan bahawa mod fonon optik membujur (LO) dalam $In_xGa_{1-x}N$ berubah dengan ketara oleh kesan gandingan LO dengan plasmon (LOPC). Spektrum pantulan IR terkutub bagi InGaN berliang tidak mengesan mod Fröhlich, kemungkinan besar disebabkan penindasan oleh lembapan. Secara ringkasnya, fungsi dielektrik IR dari kedua-dua campuran ‘seperti-ampaian’' dan 'seperti-larutan' telah dikaji secara teliti dengan menggunakan spektroskopi pantulan IR transformasi Fourier. Hasil kajian tentang tingkah laku dielektrik IR yang berkait rapat dengan mod SPhP boleh digunakan dalam memodulasi sifat-sifat optik bagi peranti berasaskan SPhP III-nitrida wurtzit pada masa akan datang.

INFRARED DIELECTRIC CHARACTERISTICS OF POROUS BINARY AND TERNARY III-NITRIDES HETEROSTRUCTURES

ABSTRACT

Porosity and composition dependence of infrared (IR) dielectric function of wurtzite III-nitrides are explored theoretically and experimentally. “Suspension-like” (i.e., porous GaN) and “solution-like” (i.e., $In_xGa_{1-x}N$) mixture are employed to investigate porosity and composition dependence of IR dielectric function respectively. Although many effective medium theories (EMTs) are available in literature, selection of appropriate EMT to describe the effective dielectric response for “suspension-like” mixture remains challenging and ambiguous. Therefore, an in-depth study on the effective dielectric properties for two-component mixtures which have four possible combinations of dielectric functions is performed. A comprehensive guideline for selecting the EMT to describe the effective dielectric behaviour of “suspension-like” mixture is proposed. Subsequently, polarized IR reflectance measurements of a set of porous GaN samples (PGaN) are performed to investigate the best EMT in describing the PGaN system as well as the impact of porosity on effective dielectric function. The reflectance spectra of PGaN can be fully described by factorized-Rayleigh (Ra) model which is developed for the first time to account for the damping of Fröhlich modes. Two weak Fröhlich modes are detected in the *s*-polarized IR reflectance spectra of PGaN at 710 cm^{-1} and 730 cm^{-1}. This implies that two additional surface phonon polariton (SPhP) modes are expected to appear in *p*-polarized IR attenuated total reflection spectra of PGaN. Besides, a red shift of SPhP mode of PGaN with increasing porosity can be predicted using factorized-Ra model. The composition dependence of the optical phonon behaviour is verified using wurtzite ternary $In_xGa_{1-x}N$/*c*-sapphire heterostructures with both flat

and porous surface morphology. The extracted E_1 lattice vibration modes of flat $In_{0.92}Ga_{0.08}N$ agree well with prediction of modified random element isodisplacement (MREI) model. For wurtzite ternary $In_xGa_{1-x}N$ (x = 0.174, 0.477, 0.719, and 0.883) with porous morphology, the MREI-predicted transverse optical phonons are in good agreement with the experimental data. Such agreement suggests that MREI model which considers only nearest neighbour's interaction sufficiently describes the composition dependence of optical phonon modes for $In_xGa_{1-x}N$ mixed crystals. In addition, result reveals that longitudinal optical (LO) phonon modes of the $In_xGa_{1-x}N$ are significantly altered by LO phonon-plasmon coupling effect. There is no Fröhlich mode detected in the polarized IR spectra for porous InGaN samples as the modes are likely suppressed by damping. In summary, IR dielectric functions of both "suspension-like" and "solution-like" mixtures are studied thoroughly using the Fourier transform infrared reflectance spectroscopy. The findings of IR dielectric behaviour which are closely related to the SPhP modes can be employed in tailoring the optical properties of wurtzite III-nitride SPhP-based devices in future.

CHAPTER 1

INTRODUCTION

1.1 Motivation

In year 2014, the Nobel Prize in Physics was awarded jointly to Isamu Akasaki, Hiroshi Amano and Shuji Nakamura for the invention of efficient blue light-emitting diodes (LEDs) based on III-nitride semiconductors (Heber, 2014). III-nitride semiconductors, namely aluminium nitride (AlN), gallium nitride (GaN), indium nitride (InN) and their alloys are the promising candidate for various optoelectronic devices from infrared (IR) to ultraviolet (UV) spectral region. These materials have wide direct band gap which spans the range from 0.64 eV (near IR) for InN (Wu, 2009), 3.4 eV (visible) for GaN (Beach et al., 2002) to 6.0 eV (near UV) for AlN (Feneberg et al., 2010). Band gap engineering or alloy composition tuning enable the realization of various devices to the wavelength of interest, such as laser diodes (Wierer and Tsao, 2015), LEDs (Khan et al., 2008), tandem solar cells (Sayad, 2016), thermoelectric material for power generation and solid-state cooling (Pantha et al., 2008). With their superior properties of high mechanical stability, high thermal conductivity, high breakdown field and strong chemical bonds, III-nitrides are more suitable for high power, high voltage, high temperature devices working in harsh environment (Lin et al., 2010; Son et al., 2010) compared to conventional semiconductors such as silicon (Si) germanium (Ge) and gallium arsenide (GaAs). Such outstanding characteristics also lead to the commercial production of electronic components, i.e., high electron mobility transistors and metal oxide semiconductor field effect transistors.

III-nitrides have drawn most of the attention and achieved a great success in two key spectral regimes, i.e., UV and visible region. Mature growth technology and higher control over interface quality have paved the way for the use of intersubband (ISB) transition to access a new spectral regime: Terahertz (THz), equivalent to the spectral region from mid-IR to far IR. The large conduction band offset (about 1.8 eV for GaN/AlN) and sub-picosecond ISB scattering rate of III-nitride heterostructures render them appealing candidates for ultrafast photonic devices operating at optical-fiber telecommunication wavelengths (near infrared) (Beeler et al., 2013; Monroy et al., 2006). In addition, III-nitrides exhibit short ISB absorption recovery times (~150 - 400 fs) due to the strong electron-phonon interaction within the material (Monroy et al., 2006). With such strength, GaN/AlN in the form of quantum wells or quantum dots becomes the potential active medium for all-optical switches operating a Tbit/s data rates and at telecommunication wavelengths (Beeler et al., 2013). Besides, large energy of GaN longitudinal-optical (LO) phonon (92 meV) opens prospects for high temperature quantum cascade lasers and ISB devices covering the IR band that was typically inaccessible to arsenide-based ISB devices due to phonon absorption (Beeler et al., 2013). Thanks to their unique material properties, the development of III-nitride optoelectronics has continued to increase recently especially for ISB devices in the IR regime such as electro-optic modulators (Liu at al., 2016), resonant tunneling diodes (Suzuki et al., 2010), IR photodetector (Qian et at., 2016) and quantum cascade laser (Scalari et al., 2003; Scalari et al., 2009). Reststrahelen band gap engineering is one of the key components in designing the IR optoelectronic devices. The information of reststrahlen band is ‘stored’ in the IR dielectric function of the material.

Miniaturization in optoelectronics and microelectronics is preferred in current technology's trend due to the desired properties such as high speed, low voltage and power of electronic component. The size shrinkage of electronic components as well as their respective devices also promotes cost saving. Nevertheless, the fundamental problem in the field of nanophotonics is to circumvent the diffraction limit of light in the optical region which obstructs the localization of electromagnetic (EM) wave into the nanoscale electronics (i.e., much smaller than the wavelength of light) (Bian, 2017; Caldwell et al., 2016). Polaritons are the quasiparticles formed by the interaction between the photons and polar excitation in the material, which can be utilized to overcome the diffraction limit. Surface plasmon polariton (SPP) and surface phonon polariton (SPhP) are the two essential examples of the polariton system. They are surface EM waves which propagate along the interface between a dielectric material having negative dielectric function and a medium having positive dielectric function. At such interface, screening of EM wave due to the coherent motion of charges results in high reflectivity and hence shows the properties of nanoscale waveguiding (Caldwell et al., 2016). Both polaritons exhibit evanescent character (confined to subdiffraction length scales near the interface) and support both localized and propagating surface modes (Spann et al., 2016). Early research of light confinement at nanoscale focused on SPPs in metals, such as silver and gold. SPP has broad bandwidth as it can be stimulated below the plasmon frequency of metal, i.e., where the dielectric function is negative in this vicinity. However, the absorption in metals limits the light to propagate only within a few micrometers and subsequent thermal issue hinders dense photonic integration (Jahani and Jacob, 2014). SPhP in polar dielectrics such as SiC and III-nitrides then appears as an attractive alternative to plasmonic material due to their long phonon lifetime (~1 - 100 ps)

(Caldwell et al., 2016). Polar material has low optical loss and operates from mid-IR to THz spectral region, but SPhP is excited only within the narrow reststrahlen band [between the transverse optical (TO) and LO modes]. Considering the pros and cons, hybrid plasmon-phonon polaritonic system which combines the benefits from both SPhP and SPP seems to be a better solution. It is worth to mention that the hybrid polariton also suffers from the decrease in optical loss and propagation length. Nevertheless, the overall performance of the hybrid is better than the pure polariton. Such hybrid system can be achieved by doping the polar dielectric heavily. The SPhP mode in polar dielectric is highly sensitive to the carrier concentration (Cheah et al., 2015; Spann et al., 2016). Therefore, active tuning and modulation of SPhP mode or the hybrid mode can be realized by changing the carrier density in the dielectric. The coupling between LO phonon and the plasmon results in a blueshift in LO phonon edge with shallower slope. Apart from tuning the carrier concentration, SPhP modulation can be achieved by tailoring the porosity of a polar semiconductor or by tailoring the alloy composition of a ternary mixed crystal.

Dielectric function is a prerequisite property to determine the SPhP mode of III-nitrides. However, investigations of IR dielectric properties of porous III-nitride and its alloy (in particular InGaN) are relatively scarce. For porous III-nitrides, most of the investigations have focused on Raman characterization only although IR spectroscopy gives rich physics associated with porosity-induced modes. While for InGaN alloy, the compositional dependence of its dielectric function remains unclear mainly due to lack of In-rich III-nitrides samples. In this dissertation, in-depth experimental and theoretical studies of the IR dielectric properties of wurtzite III-nitride heterostructures with different porosities and compositions will be performed.

1.2 Problem statements

1. The dielectric function of porous material is usually described by effective medium theories (EMTs) such as Maxwell Garnett and Bruggeman models. Despite the availability of various EMTs in literature, appropriate EMT that can reasonably describe IR-dielectric response of porous ionic crystal remains unclear.

2. Most of the related works are devoted to Raman characterization of GaN nanorod. There is lack of comprehensive investigation on the dielectric response of the GaN associated with the morphology of cylindrical air column likely due to immature fabrication technique for porous GaN (PGaN).

3. Previous experimental investigations of lattice dynamic of $In_xGa_{1-x}N$ semiconductors were mostly done on A_1(LO) and E_2 phonon modes, which are usually probed by Raman spectroscopy. Hitherto studies of E_1 phonon modes were limited to only Ga-rich $In_xGa_{1-x}N$ samples with In composition range of $0 \leq x \leq 0.3$. In other words, characterizations of E_1 phonon modes of $In_xGa_{1-x}N$ with full In composition range are highly demanded.

1.3 Objectives

- To study four possible combinations of dielectric function, in particular two-component mixture, for describing the effective optical properties of the mixture.
- To investigate the best EMT that can describe the IR dielectric response of PGaN/sapphire heterostructure.
- To study compositional dependence of E_1 optical phonon modes for wurtzite In-rich $In_xGa_{1-x}N$/sapphire heterostructure.

1.4 Scope of work

III-nitrides which possess negative dielectric function in the IR spectral region, where SPhP exist, are the potential material for SPhP based devices. IR dielectric function of III nitrides, the key parameter which modulates the SPhP, is studied based on two aspects, namely porosity and composition.

To achieve first objective, various EMTs model, namely Maxwell Garnett (MG), Inverse-Maxwell Garnett (Inv-MG), Bruggeman (BG), Lichtenecker (LTNK), Looyenga (Loo) and Rayleigh (Ra) are investigated thoroughly. The peculiar features of each model are compared systematically. Based on the findings, the best EMT model is used to describe the IR characteristics of PGaN with different porosities theoretically. Experimental data are obtained using oblique-incidence polarized IR reflectance technique. Comparison between simulation and experimental data are made then.

Theoretical platform of modified random element isodisplacement (MREI) model are developed to investigate the compositional dependence of optical phonon modes for ternary mixed crystal. The simulation is adopted to identify the mode behaviour of ternary III-nitride mixed crystals for composition range of $0 \leq x \leq 1$. The E_1 optical phonon modes for wurtzite $In_xGa_{1-x}N$/sapphire heterostructure ($x = 0.174$ to 0.883) are obtained from the previous calculation. The optical phonon modes are subsequently used to calculate the dielectric function and the IR reflectance spectrum. Comparison between simulation and experimental IR reflectance spectrum are then used to verify the mode behaviour wurtzite $In_xGa_{1-x}N$ samples.

Simulation software in the form of graphical user interface (GUI) has been compiled to ease the simulation of IR reflectance spectrum. The software can be used to calculate the polarized reflectance of multilayer system. The material parameters including thickness, dielectric constant, optical phonon modes, plasmon mode, porosity, Fröhlich mode, and depolarization factor of each layer can be extracted. To ease the discussion, the symbols of ε' (i.e., single prime) and ε'' (i.e., double prime) are used to indicate the real part and the imaginary part of dielectric function, ε.

1.5 Originality of the research

Although many EMT models are available in literature, selection of appropriate EMT to describe the effective optical response for heterogeneous system of interest remains challenging and ambiguous. Through intensive investigation, an overview of the four possible combination of dielectric function for a two-component mixture has been obtained. Such guideline will ease the selection of EMT to describe different type of two-component inhomogeneous system.

As mentioned earlier, there is only limited reported work on IR dielectric response for PGaN. Detailed characterization of optical properties for PGaN/sapphire with different porosities was performed on the basis of comparison between various EMTs. A factorized-Ra model is developed for the first time to account the individual Fröhlich damping as well as the coupling interaction between Fröhlich and plasmon mode. This model is the best model to describe the PGaN/sapphire thin film heterostructure.

A GUI-based curve fitting programme which simulates the polarized IR reflectance spectrum is extended by adding most relevant EMTs, namely MG, MG with Fröhlich damping, Inv-MG, BG, Loo, LTNK and Ra models. This new GUI can

be used for the samples with different porosities and ellipsoidal shapes. In addition, the applicability of the algorithm of Vinogradov et al. (2008) which is used to choose the correct root of BG quadratic equations has been extended to arbitrary ellipsoidal shape inclusion. Lastly, the composition dependence of E_1 modes of In-rich $In_xGa_{1-x}N$/sapphire thin films heterostructure (x = 0.174 to 0.883) was reported.

1.6 Organization of the dissertation

Chapter 1 elucidates the stimulus and inspiration of the present research. Chapter 2 firstly describes the origin of Fröhlich mode, i.e., a key idea that leads to the evolution of EMTs. This is followed by the EMTs' application on material with different type of dielectric function. A brief review of Fröhlich mode for GaN nanostructure and an overview of research on the optical phonon mode of $In_xGa_{1-x}N$ are given. Chapter 3 presents the theoretical models of dielectric function for flat semiconductors heterostructures. The second part of the chapter describes the theoretical formulae of various EMTs. Chapter 4 lists all the samples details as well as the theoretical and experimental characterization details. This is followed by the details of software implementation. Chapter 5 presents the theoretical effective dielectric response for the mixture with four different combinations of dielectric function. This is followed by the investigation of effective dielectric response of wurtzite PGaN thin film heterostructure from both theoretical and experimental aspects. Chapter 6 discusses the application of MREI model for ternary III-nitride crystals. The chapter ends with the investigation of IR reflectance spectra for both flat InGaN and porous InGaN thin film heterostructures. Finally, important results of this dissertation are summarized and some suggestions for future research are proposed.

CHAPTER 2

LITERATURE REVIEW

2.1 Introduction

This chapter begins with a brief introduction of the origin of Fröhlich mode for the finite crystals as this idea leads to the earlier development of EMTs. It is followed by the history in application of both approximation methods (i.e., EMTs) and exact methods for the mixture which consists of small inhomogeneity. Lastly, the chapter presents the literature review of Fröhlich mode for GaN nanostructures and the overview of research on the optical phonon mode of $In_xGa_{1-x}N$.

2.2 Origin of Fröhlich mode

Long wavelength dielectric functions of ionic crystals are valid for homogeneous samples. However, at the long wavelength limit, the presence of long-range Coulomb forces in finite ionic crystals causes its dielectric properties exhibit size and shape dependence (Ruppin and Englman, 1970). The definition of the finiteness is related to the comparison between the crystal dimension and the wavelength of incident light. Large crystal will absorb photon at TO while the absorption for small crystal occur at the frequencies, ω_s (surface mode) which lie between the TO and LO of the bulk material. There are two different approaches to determine the surface modes in finite crystal: (a) continuum theory (Fröhlich, 1949; Genzel and Martin, 1972a; Ruppin and Englman, 1970) and (b) exact calculation of eigenvalues and eigenvector for the lattice dynamical matrix (Genzel and Martin, 1972b; Ruppin and Englman, 1970). Although the former method neglects the

atomicity of the lattice, the theory describes long wavelength vibrations well. Hence, the theory is suitable to analyze the IR absorption for small crystals. The latter is limited to the system with small number of atoms but it is not limited to the long wavelength vibrations (Genzel and Martin, 1972b). Fröhlich (1949) is the pioneer in using continuum theory to study the effective dielectric behaviour of inhomogeneous system. He has formulated the optical phonon mode of a small spherical specimen which is embedded in the air. The particular phonon mode of small crystal is named as Fröhlich mode. The existence of Fröhlich mode is due to the increase in polarization charge on the surface of the specimen (Genzel and Martin, 1972a). Englman and Ruppin (1968) has extended the work using Mie's theory to calculate the dielectric properties for several important shape of finite crystals, namely spherical, spherical shell, cylindrical, cylindrical shell and slab. It is worth to mention that his formula (with the inclusion of retardation effect) can be applied to the specimen with arbitrary size. A general deduction can be obtained from their work: surface mode is curl-free and divergence free. In other words, the surface modes exhibit neither transverse nor longitudinal nature. Surface mode depends on the shape of the crystal and lies within the reststrahlen band (TO < ω < LO). In fact, the negligence of the retardation effect in lattice dynamical approach (Ruppin and Englman, 1970) which is parallel to Fröhlich's assumption yield the same Fröhlich frequency when the integer value for spherical Bessel and Hankel function, $l' = 1$. Fröhlich mode, ω_F is the lowest order ($l' = 1$) for the surface mode series of spherical specimen. Such mode possesses constant amplitude of vibration (or polarization) throughout the whole volume of the sphere. Although Fröhlich mode is not surface localized vibration as mentioned, it is generally called as surface mode because it is deduced under the surface mode framework. For higher orders ($l' = 2, 3$ ...), the

vibration amplitude reduces as $R^{l'-1}$ (R is the radius of the sphere) with increasing distance from surface. For small crystal, Fröhlich mode dominates. When the radius of the sphere increases, the amplitude of the Fröhlich mode peak reduces, and the peaks which originated from higher order appear and dominate. Again, Fröhlich theory can explain the long wavelength optical phonon mode appropriately as long as the crystal is small enough compared to the light wavelength.

In general, for small ellipsoid with its dimension much smaller than the incident light wavelength, the existence of Fröhlich mode with uniform polarization over the whole volume of crystal of arbitrary shape is ruled by the condition (Ruppin and Englman, 1970):

$$\varepsilon(\omega_{\mathrm{F}}) = \varepsilon_{\mathrm{m}}\left(1-\frac{4\pi}{N_{\mathrm{p}}}\right), \tag{2.1}$$

where ε_{m} is the dielectric function of the host material and N_{p} is the depolarization factor. Note that N_{p} (sphere) = $4\pi/3$, N_{p} (cylinder, long axis) = 0, N_{p} (cylinder, long axis) = 2π, N_{p} (slab, normal) = 4π and N_{p} (slab, in plane) = 0.

2.3 Application of effective medium theory on different dielectric systems

The idea in section 2.2 can be extended to the system with a distribution of the finite crystals embedded in a medium. When the effective wavelength of the radiation in the composite λ_{eff}, is much larger than the structure dimension of the inclusion a, ($a/\lambda_{eff} < 1$), the field solutions can be approximated to the electrostatic one (Qi, 2011). In such quasi-static limit, the composite can be averaged as a homogeneous medium through homogenization. Furthermore, an extra criterion has to be fulfilled for the mixture which is exposed to the time-dependent EM field. The crystallite size should be smaller than the skin depth δ (i.e., the EM wave cannot penetrate beyond the depth), so that retardation effect is negligible (Sihvola, 1999). For semiconductor, the absorption tends to occur at about 1000 cm^{-1} (i.e., far and mid-IR region), the corresponding $\delta > 1$ μm (Perkowitz, 2012). On the other hand, the condition can be satisfied for the small metal spheres with size of 20 - 30 nm in the visible and lower frequency region (Levy and Stroud, 1997).

Homogenization of a heterogeneous material is an averaging process to characterize some of its macroscopic properties in a less rigorous yet more efficient manner than the full microscopic description (Qi and Sihvola, 2011). For instance, dielectric variation for a whole microstructure can be averaged to effective dielectric function (ε_{eff}') using homogenization theories (Sihvola, 1999). Particularly, investigation on homogenization theories which evaluates the effective dielectric properties of inhomogeneous material has been started by Mossotti, Clausius, Lorenz, Lorentz and Rayleigh since 19^{th} century (Sihvola, 2013). Subsequently, various EMTs evolved from these pioneering works.

There are several significant EMTs, namely MG (Maxwell Garnett, 1906) model, BG (Bruggeman, 1935), unified mixing model (Sihvola, 1999), and power law (PL) (Birchak et al., 1974; Lichtenecker, 1996; Looyenga, 1965). The difference between the EMTs originated from their assumption of topology of the composite and the way how the interaction among the constituents is taken into account. MG model is widely used for ordered lattice material such as silicon carbide (SiC) (Spanier and Herman, 2000), metal nanoparticle in polymer (Faupel et al., 2010; Takele et al., 2006) and ceramic-metal composite (Ahn and Roper, 2008). BG model is suitable to describe the amorphous material (Böttcher and Bordewijk., 1978) such as amorphous GaAs (Adachi, 1991) and snow (Mazeh et al., 2016). In addition, BG formula is also used in the area of geophysical sensing (Bartlett et al., 2017; Cosenza et al., 2009). Loo model, one of the family members of PL, is only valid for low contrast between the inclusion and the host. Loo formula is not appropriate to describe metal-insulator composite (Merrill et al., 1999), but it is appropriate for dielectric-dielectric mixtures, like silicate (Maron and Maron, 2008). The application of LTNK formula is mainly applied for ceramic (Buixaderas et al., 2015; Nuzhnyy et al., 2014) and graphite (Maron and Maron, 2008).

In fact, all EMTs give nearly the same description for the inhomogeneous medium in dilute limit. When concentration of the inclusion increases, EMTs start to deviate from one another due to different assumptions in microgeometry and the interaction among the constituents of a composite. In addition, the accuracy of the EMTs prediction can be greatly reduced due to the negligence of multipole interaction between the inclusions. One should compare the EMTs result with the rigorous EM simulation. However, an exact solution can only be obtained in some extreme cases where the shape, size and the position of the particles are exactly

known. In other words, no exact theoretical solution can be found for disordered system with random size, shapes and distribution of inclusions. In this case, approximation must be made. EMTs give analytical solutions for the system with ellipsoidal shape inclusions only. To analyze structures with arbitrary shape inclusion, numerical techniques such as periodic finite-difference time-domain (FDTD) method (Karkkainen et al., 2001), Fourier series expansion method (Toumelin et al., 2005), finite element method (FEM) (Sareni et al., 1996; Sun et al., 2010), separation variable, discrete dipole approximation (Maron and Maron, 2008; Zhuromskyy, 2016), transition matrix (Zhuromskyy, 2016), plane wave expansion (Volkov et al., 2012) and etc. can be adopted in the simulation of the interaction between EM field and matter.

Three decades ago, exact method is focused on the system with positive dielectric constant only. Liebsch and Persson (1983) simulated dipolar interactions in a random suspension using lattice-gas model. But, the approach considers the dipole approximation only. Doyle and Jacob (1990) then developed an effective cluster model which takes account of the multipole interaction to explain the inhomogeneous medium, i.e., oil with high volume fraction of mercury (Hg) inclusion. Their exact calculation gives excellent agreement with experiment data. Merrill et al. (1999) adopted Doyle's method to study the lossy medium in which spherical carbonyl iron powder embedded in the continuum of rubber. The ε_{eff} is frequency-dependent as inclusion is dispersive. At 'DC' limit (i.e., independent of time), the predictions of both Doyle's method and iterative asymmetric-Bruggeman (A-BG) model coincided with experiment. At frequency of 4 GHz, A-BG model is superior among other EMTs to describe the system with multiple sizes of metallic spheres in dielectric host continuum when percolation threshold is suppressed. Sun et

al. (2010) who was inspired by Doyle's work simulate the ε_{eff} of composite material (ε_1 = 1, ε_2 = 16) based on the FEM and S-parameters retrieval algorithm. The ε_{eff} with regular square lattice array of inclusion is independent of frequency and lossless. Yet, when the non-overlapping inclusions are randomly arranged, the ε_{eff}' increases with frequency. This may be due to Mie resonance. The result is astonishing because the ε_{eff} is dispersive and lossy although both the inclusion and the host are frequency-independent and lossless. In addition, the results revealed the prediction of MG model agrees well with the FEM calculation for the case of regular or periodic inclusions. When the inclusions are randomly positioned, the calculated result deviates from MG model results. Nevertheless, the result still lies between the MG and BG curves.

If the composite has matrix topology, it can be treated in two ways: (a) raisin pudding and (b) Swiss cheese. Karkkainen et al., (2000) is one of the pioneers in applying FDTD to solve the ε_{eff} of lossless composite (ε_1 = 1, ε_2 = 16). In the simulation, clustering is allowed. The inclusion is randomly distributed and the size is not uniform but within quasistatic limit. Based on the low frequency simulation, the electric field is attenuated inside inclusion in raisin pudding mixture. While in Swiss cheese mixture, there is an increase in field strength. For samples which has random inclusion with real dielectric, there is no single individual model can globally agree with the FDTD calculations. The numerical simulation result lies between BG and MG curves for both configurations. In contrast to Karkkainen et al.' simulation, Volkov et al., (2012) used plane-wave expansion method to simulate ε_{eff} of composite with non-overlapping cylinders. The composite consists of bulk Si dielectric with dielectric constant = 11.9 and air which are arranged in both Swiss cheese and raisin pudding geometry. For each of the geometry, ordered and random

distribution of holes (Swiss cheese) and rods (raisin pudding) are considered. In this case, MG theory gives a good description of periodic photonic-crystal samples, especially arranged in triangular lattice for both rods and holes with volume fraction up to about 60%. The deviation between the calculation and MG results increases when the distance between the neighbouring cylinders decreases. The closer the cylinders, the stronger the localized field, and hence the larger the deviation is claimed. In the case of overlapping of cylinders is allowed, BG formula is also adopted as the sample microgeometry tends to approach BG's topology when overlapping is allowed. The numerical calculation is in between MG and BG limits for both rod- and hole-based 2D samples.

With the advent of metamaterial and its novel EM properties, the focus of the homogenization theory has been extended to the composite with negative dielectric function since last decade. Fourn and Brosseau (2008) have investigated the impact of dielectric contrast between the host dielectric and the inclusion dielectric on the ε_{eff} of the heterostructure and the impact of inclusion shape on the electrostatic resonance (ER) position. Finite element based simulation is performed for three cases (a) ε_i is positive and real, (b) ε_i is complex, and (c) ε_i is complex but its real part is negative, where ε_i is the dielectric function of inclusion. The composite is two-dimension with positive ε_m' for all cases. The inclusions are not allowed to overlap. In cases (a) and (b), the numerical calculation tends to have a better agreement with MG model compared to the BG model for both Swiss cheese and raisin pudding configurations. Figure 2.1 plots the local electric field profile around the inclusion. From Fig. 2.1, local electric field enhancement which is due to the applied field occurs for all three cases though at different vicinity around the inclusion. Hence, this goes against the criteria of the mean field theory or EMT

assumptions where the field is uniform. This contributes the discrepancy between the numerical data and the EMT's prediction. In case (c), MG model predicts well the ER position even when the inclusion concentration is beyond the dilute limit but BG model fails to gives the correct ER position. ER can be understood as Fröhlich mode in this dissertation. Mackay and Lakhtakia (2004) also suggest that BG model is inappropriate for the composite material having dielectric component with $\varepsilon_i' \varepsilon_m' < 0$.

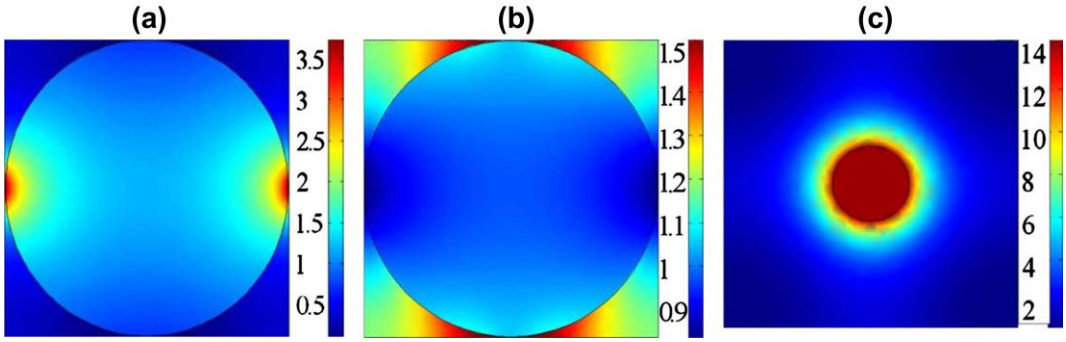

Fig. 2.1: Local electric field enhancement factor $|\mathbf{E}(\mathbf{r})|/E_0$ for the 2D composite structure consisting of a circular inclusion in the matrix: (a) $\varepsilon_2 = 1$ and $\varepsilon_1 = 10$; $f = 0.782$, (b) $\varepsilon_2 = 1 + i$ and $\varepsilon_1 = 1$; $f = 0.782$, and (c) $\varepsilon_2 = -10 + i$ and $\varepsilon_1 = 10$; $f = 0.053$. In all three cases, medium 2 is embedded in the host component medium 1. $|\mathbf{E}(\mathbf{r})|/E_0$ denotes the norm of the local electric field (the applied electric field) while f denotes the volume fraction of the inclusions. Reprinted figures with permission from [C. Fourn and C. Brosseau, Phys. Rev E, 77, 016603, 2008]. Copyright (2017) by the American Physical Society.

MG formula predicts one singularity while the Rayleigh formula predicts two singularities with good accuracy compare to the exact calculation for a square lattice when the inclusion concentration is low. BG model does not predict any singularities, but gives a complex ε_{eff} even both the constituents ε are real. Detailed discussion on

the peculiar prediction of each model will be presented in the Chapter 5. Wallén et al., (2009) discussed the limitations and compared the applicability of MG and Rayleigh models in two dimensions with FEM calculation of ε_{eff}' for plasmonic mixture (silver nanorod in air) with cylindrical inclusions in a regular and slight disordered lattice (Wallén at al., 2009). In their simulation, the cylinders are not allowed to overlap. Comparing the numerical result, Rayleigh formula give accurate results for composite even at high volume fractions of inclusion (i.e., up to 50 %) while MG is accurate up to volume fraction of 25 % only. Rayleigh formula is the refinement of MG model because it takes account of higher order of multipole interaction between the inclusions. Nevertheless, none of the mixing rule is accurate when the cylinders are almost touching each other, because many singularities and higher order interaction are neglected in these formulas. Near the plasmonic resonances, the accuracy of Rayleigh formula decreases significantly when the lattice is slightly distorted. However, as long as the cylinder are not allowed to be too close to each other, MG and Rayleigh formula still able to give useful and qualitative estimate of the ε_{eff}' of the composite. To ease the reading, the important remarks for each of the literature have been systematically tabulated in Table 2.1.

Table 2.1: Literature review of application of EMTs on different dielectric composite.

Author (Year)	Numerical method (NM)/EMTs	Material	Remarks
Lossless and lossy composite			
Liebsch and Persson (1983)	NM: - lattice-gas model EMT: - MG	Ag particles immersed in gelatin $\varepsilon_m = \varepsilon_{gelatin} = 2.37$ $\varepsilon_i = \varepsilon_{Ag}$	- The particle assumed to occupy at random at the sites of a fictitious crystal structure. - Coherent potential approximation is used to evaluate the contribution to the local field which is caused by the randomly located particles. However, only dipole part of the field is considered. - Both theoretical approaches, namely lattice-gas model and MG model fail to match well with experimental data.
Doyle and Jacob (1990)	NM: - effective cluster model EMT: - Clausius-Mossotti relation	Hg droplets in oil $\varepsilon_m = \varepsilon_{oil} = 2.263$ $\varepsilon_i = \varepsilon_{Hg}$	- High electric multipole interactions are taken into account. - The system is modeled as a disordered monodispersed suspension, or a mixture of isolated spheres of uniform sized and closed-packed spherical clusters of spheres. - The effective cluster model is in excellent agreement with the experimental dielectric constant and conductivity measurements up to the volume filling factor =0.45.
Merrill et al. (1999)	NM: - Doyle-Jacob (D-J) method	Mixture of carbonyl-iron powder (CIP) and rubber at DC limit and 4GHz	- At DC limit, the prediction of both (D-J) and A-BG match well with the experimental result

	EMT: - A-BG - BG - MG - Loo	$\varepsilon_m = \varepsilon_{rubber}$ $= 2.43 - j0.029$ $\varepsilon_i = \varepsilon_{CIP}$ $= 1.0 - j\sigma/\varepsilon_0\omega$	- At 4GHz, A-BG gives the best qualitative prediction of ε_{eff} among other EMTs.
Sun et al. (2010)	NM: - FEM and S-parameters retrieval algorithm EMT: - BG - MG	Mixture of lossless host material and lossless circular particle inclusions $\varepsilon_m = 1$ $\varepsilon_i = 16$	- When the inclusions are arranged in regular lattice, ε_{eff}' of the mixture is independent of frequency and lossless. The ε_{eff}'agrees well with MG prediction. - When the inclusions are randomly positioned, the real part of the ε_{eff}' increases with frequency. The ε_{eff}' deviate from MG results, but still tend to approach MG curve in the case of no overlapping of inclusions is allowed.
Lossless dielectrics which are arranged in both raisin pudding and Swiss cheese configuration			
Kärkkäinen et al., (2000)	NM: - FDTD EMT: - BG - MG - Coherent potential formula - PL	(a) Raisin Pudding $\varepsilon_m = 1$ $\varepsilon_i = 16$ (b) Swiss Cheese $\varepsilon_m = 16$ $\varepsilon_i = 1$	- Overlapping of the inclusion particles are allowed in simulation for both configurations. - The numerical result lies between the BG and MG curves for both configurations. - It is worth to mention that there is no single model can describe the mixture with random inclusion, all values lies between the Wiener Limit.
Volkov et al., (2012)	NM: - plane wave expansion method	(a) Raisin Pudding $\varepsilon_m = 1$ $\varepsilon_i = 11.9$	- The work can be separated into two parts: (a) No overlapping of inclusion is allowed (b) Overlapping of inclusion is allowed.

	EMT: - BG - MG	(b) Swiss Cheese $\varepsilon_m = 11.9$ $\varepsilon_i = 1$	(a) Non-overlapping case - MG agrees well with numerical calculation for the samples with inclusion arranged in triangular lattice up to high volume fraction. (b) Overlapping case - MG curve deviates more from the numerical result compared to that of non-overlapping case. - Allowing the cylinder to overlap, the sample micro-geometry is closer to a symmetric matrix of the dielectric and the air. - The numerical calculation is in between MG and BG limits for both raisin pudding and Swiss cheese configuration.
Composite with negative ε_i'			
Fourn and Brosseau (2008)	NM: - FEM EMT: - MG - BG	ε_m is positive and real Case 1 ε_i is positive and real Case 2 ε_i is complex Case 3 ε_i is complex but its real part is negative	- The composite is arranged in raisin pudding configuration Case 1 - The calculation tends to agree with MG compared to BG result. - There is field enhancement within the inclusion due to the applied field. Case 2 - Compared to BG, MG gives better agreement with numerical result. - The inclusion inside the inclusion is not uniform, but more prominent field enhancement occurs outside the inclusion.

			Case 3 - MG is able to predict the ER position when the volume fraction of the inclusion is small. - For symmetric BG model, the assumption of the homogeneous local field in each component of the composite lead the failure of BG model in describing the optical properties of material with negative ε_i'.
Wallén et al., (2009)	NM: - FEM EMT: - MG - BG - Ra	- Mixture of air and a plasmonic material with negative ε_i' - Silver-air composite in raisin pudding configuration	- The cylindrical inclusions are arranged in periodic square lattice. - Overlapping is not allowed. - In a two-phase mixture, if one constituent has lossless positive ε_i', the ε_{eff} must be lie between the dielectric function of the constituents. - MG model shows one singularity and Ra gives two singularities at low volume concentration. - BG does not predict any singularities but a complex region for negative real ε_i' of one constituent. - Rayleigh formula give accurate results for composite even at high volume fractions of inclusion (i.e., up to 50%) while MG is accurate up to volume fraction of 25% only. - Near the plasmonic resonances, the accuracy of Rayleigh formula decreases significantly when the lattice is slightly distorted.

2.4 Overview of research on the Fröhlich mode of GaN nanostructure

Numerous works have been carried out to exploit the potential application of the EMTs in characterizing the effective properties of various nanostructures (Dyck et al., 2011; Wąsik et al., 2017), metamaterials (Newman, 2012; Sadeghi et al., 2015; Zhang and Wu, 2015), ceramics (Campo et al., 2014; Nuzhnyy et al., 2014) and thin film heterostructure (Montiel-González et al., 2016; Sarua et al., 2001; Spanier and Herman, 2000). In fact, EMTs are also applied to investigate the phonon properties of III-nitrides nanostructures, especially on GaN nanocolumns. In early stage of the phonon-related research for GaN nanostructures, nanostructuring-induced surface vibrations which lie between the TO and LO phonon gap were observed from Raman scattering spectra and they were assigned as Fröhlich mode (Milekhin et al., 2006; Tiginyanu et al., 2001; Yuan et al., 2003). Sekine et al. (2006) has reported the Fröhlich mode in three samples with different column densities for GaN nanocolumns and GaN/AlN multiple quantum disk nanocolumns. They adopted 2D-MG model and formula of Raman intensity to predict the filling ratio of the nanocolumns. Hsiao et al. (2007) has also reported the observation of the Fröhlich mode in a single free standing GaN nanorod by micro-Raman spectroscopy. However, detailed discussion on characterization of Fröhlich mode from these works is not sufficient. The understanding of phonon properties is crucial from the fundamental point of view and for the application of related phonon-assisted electronic devices. Investigation in-depth should be carried out for this topic which still remains poorly studied. Mata et al. (2012) used the dielectric continuum model to determine the surface optical mode of GaN nanowire. There are approximately 20 - 30 cm^{-1} discrepancy between the theoretical calculation and the experimental data. Nevertheless, they eventually demonstrated that MG model provides an

accurate description of the Fröhlich vibrational mode for their samples. Sekine et al. (2017) described the Fröhlich mode observed in the Raman scattering spectra as SPhP. The Fröhlich mode at around 705 cm^{-1} has been observed for both regularly arrayed GaN nanowalls and nanocolumns. The intensity of the peculiar mode decreases with increasing wall width, and the mode disappears at wall width of 340 nm. This indicates the localized mode originates from the *a*-plane of the nanowall. They also found that the Fröhlich peak position remains unchanged when the nanocolumn diameter was changed. According to Raman selection rules, only E_2(high) and A_1(LO) phonon modes can be observed in backscattering geometry for *c*-plane GaN surface (Jimenez and Tomm, 2016). Usually, breakdown of selection rule occurs in nanostructure. As a result, the observation of forbidden transverse A_1(TO) and E_1(TO) can always be an indicator of surface morphology of the sample.

Up to now, most of the related works devoted to Raman characterization of the Fröhlich mode for GaN nanorod. There is lack of comprehensive investigation on the dielectric response of the GaN associated with the morphology of cylindrical air column. In addition, MG model which gives good agreement with the experimental results are usually used to describe the nanostructure system without understanding the reason behind. In this work, polarized IR reflectance technique is employed to probe the optical properties of PGaN on *c*-sapphire substrate. The predictions of various EMTs on dielectric response of PGaN are compared and discussed in-depth.

2.5 Assumption of force constant in MREI model

The IR dielectric properties of a material can be changed by various ways, such as doping and changing the surface morphology of the material. Another way is to mix the material with another substance (alloying) to form a ternary mixed crystal. Optical phonon frequency, which is an important parameter of dielectric function, varies with composition for this mixed crystal. Compositional dependence of optical phonon modes for polar ternary mixed crystals can be predicted using MREI model developed by Chang and Mitra (1968). According to MREI model, besides of short range mechanical coupling force between the ions, long range local electric field force is considered to be exerted on the ions. The bonding force between the neighbour atoms plays a decisive role in determining the resonant phonon modes, i.e., quanta of the lattice vibration.

Previous studies have suggested that the ratio of nearest neighbour (NN) force constant to second nearest neighbour (SNN) force constant, r is different for each individual crystal, i.e., $Z \approx 3$ for $Zn_{1-x}Mn_xSe$ (Lao et al., 1993) and $Cd_{1-x}Mn_xTe$ (Peterson et al., 1986), $Z \approx 4$ for $Ga_{1-x}Al_xSb$ (Lucovsky et al., 1975) and $Z \approx 5$ for $Zn_{1-x}Mn_xTe$ (Peterson et al., 1986). The influence of force constant on optical phonon mode and SPhP properties of cubic $ZnS_{1-x}Se_x$ mixed crystals has been investigated theoretically (see Appendix A). With the supporting experimental data, results showed that SNN interaction is significant to determine the optical phonon mode of cubic $ZnS_{1-x}Se_x$ mixed crystals. In fact, the assumption of SNN interaction is optional in MREI model. The significance of SNN interaction can be verified only if sufficient experimental data are available to prove the existence of impurity modes, namely local mode and gap mode for the mixed crystals.